Inorganic Chemistry

pubs.acs.org/IC

Article

Selective Metal−Ligand Bond-Breaking Driven by Weak Intermolecular Interactions: From Metamagnetic Mn(III)-Monomer to Hexacyanoferrate(II)-Bridged Metamagnetic Mn_2Fe Trimer

Somen Goswami, Soumen Singha, Indrajit Saha, Abhishikta Chatterjee, Subrata K. Dey,* Carlos J. Gómez García,* Antonio Frontera, Sanjay Kumar,* and Rajat Saha*

Cite This: https://dx.doi.org/10.1021/acs.inorgchem.0c00909

Read Online

ACCESS | Metrics & More | Article Recommendations | Supporting Information

ABSTRACT: Metal−ligand coordination interactions are usually much stronger than weak intermolecular interactions. Nevertheless, here, we show experimental evidence and theoretical confirmation of a very rare example where metal−ligand bonds dissociate in an irreversible way, helped by a large number of weak intermolecular interactions that surpass the energy of the metal−ligand bond. Thus, we describe the design and synthesis of trinuclear Mn_2Fe complex $\{[Mn(L)(H_2O)]_2Fe(CN)_6\}$,$^{2-}$ starting from a mononuclear Mn(III)-Schiff base complex: $[Mn(L)(H_2O)Cl]$ (**1**) and $[Fe(CN)_6]^{4-}$ anions. This reaction implies the dissociation of Mn(III)-Cl coordination bonds and the formation of Mn(III)-NC bonds with the help of several intermolecular interactions. Here, we present the synthesis, crystal structure, and magnetic characterization of the monomeric Mn(III) complex $[Mn(L)(H_2O)Cl]$ (**1**) and of compound $(H_3O)[Mn(L)(H_2O)_2]$-$\{[Mn(L)(H_2O)]_2Fe(CN)_6\}\cdot 4H_2O$ (**2**) (H_2L = 2,2′-((1*E*,1′*E*)-(ethane-1,2-diylbis-(azaneylylidene))bis(methaneylylidene))bis(4-methoxyphenol)). Complex **1** is a monomer where the Schiff base ligand (L) is coordinated to the four equatorial positions of the Mn(III) center with a H_2O molecule and a Cl^- ion at the axial sites and the monomeric units are assembled by $\pi-\pi$ and hydrogen-bonding interactions to build supramolecular dimers. The combination of $[Fe(CN)_6]^{4-}$ with complex **1** leads to the formation of linear Mn-NC-Fe-CN-Mn trimers where two *trans* cyano groups of the $[Fe(CN)_6]^{4-}$ anion replace the labile chloride from the coordination sphere of two $[Mn(L)(H_2O)Cl]$ complexes, giving rise to the linear anionic $\{[Mn(L)(H_2O)]_2Fe(CN)_6\}^{2-}$ trimer. This Mn_2Fe trimer crystallizes with an oxonium cation and a mononuclear $[Mn(L)(H_2O)_2]^+$ cation, closely related to the precursor neutral complex $[Mn(L)(H_2O)Cl]$. In compound **2**, the Mn_2Fe trimers are assembled by several hydrogen-bonding and $\pi-\pi$ interactions to frame an extended structure similar to that of complex **1**. Density functional theoretical (DFT) calculations at the PBE1PBE-D3/def2-TZVP level show that the bond dissociation energy (−29.3 kcal/mol) for the Mn(III)-Cl bond is smaller than the summation of all the weak intermolecular interactions (−30.1 kcal/mol). Variable-temperature magnetic studies imply the existence of weak intermolecular antiferromagnetic couplings in both compounds, which can be can cancelled with a critical field of ca. 2.0 and 2.5 T at 2 K for compounds **1** and **2**, respectively. The magnetic properties of compound **1** have been fit with a simple $S = 2$ monomer with $g = 1.959$, a weak zero-field splitting ($|D| = 1.23$ cm^{-1}), and a very weak intermolecular interaction ($zJ = -0.03$ cm^{-1}). For compound **2**, we have used a model with an $S = 2$ monomer with ZFS plus an $S = 2$ antiferromagnetically coupled dimer with $g = 2.009$, $|D| = 1.21$ cm^{-1}, and $J = -0.42$ cm^{-1}. The metamagnetic behavior of both compounds is attributed to the weak intermolecular $\pi-\pi$ and hydrogen-bonding interactions.

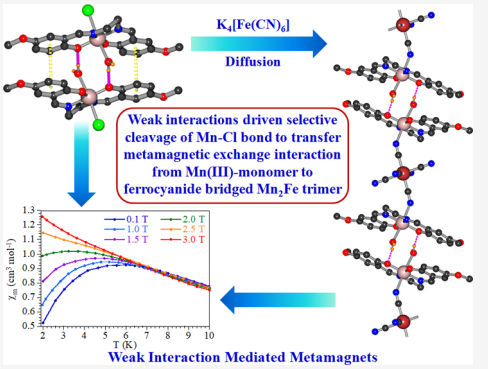

INTRODUCTION

Selective bond making−bond breaking is the finest art of chemistry and has tremendous significance in molecular and supramolecular chemistry.[1−4] After a prolonged research over centuries, chemists have gained mastery over covalent and metal−ligand coordination bond breaking−bond making processes, whereas control over the supramolecular interactions is still a daunting task. Several catalytic processes[5−9] are well-known for the selective bond activation, bond breaking, and bond making in organic chemistry. In coordination chemistry, the so-called *trans* effect,[10,11] the HSAB principle,[12,13] etc. can successfully explain the selective metal−ligand bond breaking−bond making process. In supramolecular chemistry, molecular recognition and aggregation constitute

Received: March 27, 2020

the base of selectivity and determine the final compound and strucutre.[14−18] Supramolecular interactions are much weaker than covalent/coordinate bonds and therefore a minor chemical or physical perturbation may cause a severe change in the weak interaction network of the system. Here, we present a case study where weak interactions drive a metal−ligand coordination bond dissociation during the formation of a hexacyanoferrate(II)-bridged Mn_2Fe trimer from a Mn(III)-monomeric precursor.

In molecular magnetism, metamagnets[19−22] are a special type of magnetic material in which two magnetic motifs (which may be a molecule, a one-dimensional (1D) chain, or a two-dimensional (2D) layer) interact antiferromagnetically (AF) through weak intermotif (molecule or chain or layer) interactions and the application of a DC field above a certain critical field (H_C) can alter this weak AF coupling into a ferromagnetic (FM) one at low temperatures (T_N).[23,24] Such coexistence of AF and FM in a material is difficult to predict and, consequently, highly challenging to design, but it may have significant applications in technologies associated with magnetic cooling[25] and the magnetocaloric effect.[26] This magnetic-field-induced first-order transition from AF to FM is critically dependent on the weak intermotif interactions. Mukherjee et al.[22] have reported that the metamagnetism arises due to weak C−H···N hydrogen-bonding interactions between azido-bridged 1D coordination chains of Ni^{II}−Schiff base complex. Chen et al.[27] have reported the metamagnetic behavior of 2-fold interpenetrated coordination layers, where weak hydrogen bonding and dipolar interactions between adjacent layers are responsible for such metamagnetic transition. Ghosh et al.[28] reported metamagnetism due to weak interchain C−H···N hydrogen bonding between neighboring coordination chains formed by Mn(III)-tridentate Schiff base units connected with azide ligands in its *end-on* (μ-1,1′) coordination mode. Therefore, to design a metamagnetic material, we must control the weak intermolecular interactions, although, due to the difficulty involved with this control, most of the reported molecular metamagnets are basically serendipitous. With this background, we have designed a strategy to prepare molecular metamagnets through controlled breaking of metal−ligand bonds helped by the cumulative functions of a large number of weak interactions.

In the past few years, high spin Mn(III)-Schiff base complexes have been used as structural building units to design several types of magnetic materials, such as single-chain magnets[29,30] (SCMs), single-molecule magnets[31,32] (SMMs), ferromagnets,[33,34] antiferromagnets,[35,36] etc., thanks to several unique properties of the Mn(III) ions: (i) stable oxidation state, (ii) high spin configuration (S = 2), (iii) easily substitutable axial sites, and (iv) unusual uniaxial anisotropy (D) arising from Jahn−Teller distortion in octahedral geometry.

In this context, we have synthesized a Mn(III) complex with a N_2O_2 donor-based Schiff base ligand and studied its structure and magnetic properties. X-ray structural study reveals Mn(III)-monomeric units with axial water and chloride ligands, that are further assembled by hydrogen bonds and $\pi-\pi$ interactions to form a supramolecular dimer with a very small intradimer antiferromagnetic coupling and a metamagnetic behavior with a critical field of ca. 2.0 T at 2 K. The hard acid−soft base interaction makes the coordinated chlorides highly labile and the reaction of complex **1** with $K_4[Fe(CN)_6]$ replaces the chlorides from the coordination sphere of two adjacent monomeric Mn(III) units to yield a *trans* cyanide-bridged Mn_2Fe trimer (complex **2**) that cocrystallizes in a 1:1 ratio with a Mn(III) monomer closely related to complex **1**. Structural analysis reveals the preservation of weak intermolecular hydrogen bonds and $\pi-\pi$ interactions during the transformation of the monomer into the trimer as well as the metamagnetic behavior. These Mn_2Fe trimers are assembled by hydrogen bonds and $\pi-\pi$ interactions, giving rise to supramolecular chains that also present a metamagnetic transition with a critical field of ca. 2.5 T at 2 K.

EXPERIMENTAL SECTION

Materials and Methods. $MnCl_2{\cdot}4H_2O$ (99%), 2-hydroxy-5-methoxybenzaldehyde (99.5%), ethylenediamine (99.5%), and $K_4[Fe(CN)_6]$ (99%) have been purchased from Sigma-Aldrich and used without further purification. Triethylamine and all other chemicals (AR grade) were purchased from Merck India and used as received. A PerkinElmer 240C elemental analyzer was employed to perform elemental analysis (C, H, N). The Fourier transform infrared (FT-IR) spectra have been recorded by a Nicolet Impact 410 spectrometer, using KBr pellets in the range of 400−4000 cm^{-1}.

Synthesis of the Ligand (H_2L). The Schiff's base ligand (H_2L = 2,2′-((1*E*,1′*E*)-(ethane-1,2-diylbis(azaneylylidene))bis-(methaneylylidene))bis(4-methoxyphenol)) was synthesized (see Scheme 1, presented later in this work) by refluxing 2-hydroxy-5-methoxybenzaldehyde (10 mmol, 1.525 g) with ethylenediamine (5 mmol, 300 mg) in a 2:1 ratio in methanol (20 mL) at 90 °C for 1 h. The reaction mixture was then cooled and filtered to separate out the yellow-colored crystalline solid product, washed with diethyl ether, and dried in air. Yield: ∼90%.

Synthesis of [(L)Mn(H_2O)Cl] (1). The Schiff base ligand H_2L (165 mg, 0.5 mmol) was dissolved in 20 mL of boiling methanol and the pH of the methanolic solution was adjusted to 9 by Et_3N. An aqueous solution (5 mL) of $MnCl_2{\cdot}4H_2O$ (100 mg, 0.5 mmol) was added to the previous solution and the resulting solution was refluxed for 2 h. The reaction mixture was cooled, filtered off, and the light yellowish brown filtrate was kept undisturbed for crystallization. Brown needlelike crystals suitable for single-crystal X-ray analyses were collected after 2 weeks. Yield: ∼86%. Anal. Calc. for $C_{18}H_{20}ClMnN_2O_5$: C, 49.7; H, 4.6; N, 6.4%. Found: C, 49.8; H, 4.5; N, 6.5%. Selected IR bands (KBr pellet, cm^{-1}): ν (C═N) 1605(s); ν (O−H) 3385(broad).

Synthesis of $(H_3O)[Mn(L)(H_2O)_2]\{[Mn(L)(H_2O)]_2Fe(CN)_6\}\cdot 4H_2O$ (2). The cocrystal of this hexacyanoferrate(II)-bridged trimeric complex was synthesized via a layering technique, using the monomeric complex **1** and a $K_4[Fe(CN)_6]$ solution in a 1:1 ratio with a water−methanol buffer solution. Complex **1** (110 mg, 0.25 mmol) was dissolved in 30 mL of a 9:1 methanol−water mixture. A second solution was prepared dissolving $K_4[Fe(CN)_6]$ (108 mg, 0.25 mmol) in 25 mL of distilled water. These two solutions were layered in eight different tubes using a 1:1 water−methanol buffer and kept undisturbed for crystallization. Deep-brown needle-shaped crystals suitable for X-ray diffraction (XRD) analysis were collected after one month, then washed with hexane and dried. Yield: 79%. Anal. Calc. for $C_{60}H_{73}FeMn_3N_{12}O_{21}$: C, 47.4; H, 4.8; N, 11.1%. Found: C, 47.5; H, 4.7; N, 11.1%. Selected IR bands (KBr pellet, cm^{-1}): ν(C≡N) stretching 2123, 2105(s); ν(C≡N) 1608(s); ν(O−H) 3410(broad).

Magnetic Measurements. Magnetic measurements on compound **1** and **2** (with masses of 33.446 and 4.406 mg, respectively) were performed using a Quantum Design MPMS-XL-7 SQUID magnetometer in the temperature range of 2−300 K in the presence of an external magnetic field of 0.1 T (and in the temperature range of 2−10 K with different applied fields in the range of 0.1−3.0 T). The isothermal magnetizations were measured at 2 K with magnetic fields of up to 7 T on the same samples. The susceptibility data were corrected for the sample holders previously measured using the same conditions and for the diamagnetic contributions of the compounds, as deduced by using Pascal's constant tables.[37]

https://dx.doi.org/10.1021/acs.inorgchem.0c00909
Inorg. Chem. XXXX, XXX, XXX−XXX

Theoretical Methods. All DFT calculations included in this manuscript have been performed using the Gaussian-16 program[38] at the PBE1PBE-D3/def2-TZVP level of theory and using the crystallographic coordinates. The formation energies of the assemblies have been evaluated by calculating the difference between the overall energy of the assembly and the sum of the monomers that constitute the assembly, which have been maintained frozen. The Atoms-in-Molecules (AIM)[39] analysis has been performed at the same level of theory. The calculation of AIM properties was done using the AIMAll program.[40]

Crystallographic Data Collection and Refinement. Suitable single crystals of complexes **1** and **2** were mounted on a Bruker SMART CCD diffractometer equipped with a graphite monochromator and Mo Kα (λ = 0.71073 Å) radiation, and then the structures were solved via the Patterson method, using several software programs.[41−45] The details of the process are given in the Supporting Information file. All the crystallographic data and refinement parameters of both complexes are presented in Table 1. Complex **2** contains disordered guest water molecules.

Table 1. Crystallographic Data Collection and Refinement Parameters of Compounds 1 and 2[a,b,c]

	Value/Comment	
parameter	1	2
formula	$C_{18}H_{20}ClMnN_2O_5$	$C_{60}H_{73}FeMn_3N_{12}O_{21}$
formula weight	434.75	1518.97
crystal system	orthorhombic	triclinic
space group	P_{bca}	$P\bar{1}$
a (Å)	11.826(6)	14.0832(14)
b (Å)	12.872(7)	15.0504(15)
c (Å)	22.919(12)	17.0031(18)
α (deg)	90	108.703(3)
β (deg)	90	101.649(3)
γ (deg)	90	90.023(4)
unit-cell volume, V (Å^3)	3489(3)	3335.1(6)
Z	8	2
ρ_{calc} (g/cm^3)	1.655	1.513
μ (Mo Kα) (mm)	0.945	0.850
F(000)	1792	1572
crystal size (mm^3)	0.08 × 0.12 × 0.16	0.12 × 0.16 × 0.20
temperature, T (K)	100	152
$\theta_{min-max}$ (deg)	1.8, 25.3	2.5, 27.2
total data	28731	34615
unique data	3156	14564
R_{int}	0.177	0.126
observed data [$I > 2.0\sigma(I)$]	1625	7216
N_{ref}	3156	14564
N_{par}	244	878
R	0.0581	0.0963
wR_2	0.1195	0.2874
S	0.80	1.01

[a] $R_1 = \sum||F_o| - |F_c||/\sum|F_o|$. [b] $wR_2(F_o^2) = [\sum[w(F_o^2 - F_c^2)^2/\sum wF_o^4]^{1/2}$. [c] GooF = $[\sum[w(F_o^2 - F_c^2)^2/(N_{obs} - N_{params})]^{1/2}$

RESULTS AND DISCUSSION

Synthesis. The tetradentate Schiff-base ligand (H_2L) was synthesized by the combination of ethylene diamine with 2-hydroxy-5-methoxybenzaldehyde in a 1:2 ratio (see Scheme 1). Combination of the synthesized ligand with $MnCl_2$ leads to the aerial oxidation of Mn(II) to Mn(III) with formation of the neutral complex **1**, that, besides the ligand L^{2-}, contains one Cl^- and one water molecule at the axial sites (Scheme 1). When complex **1** is reacted with $[Fe(CN)_6]^{4-}$, the cyanide groups replace the coordinated chloride ions of two neighboring Mn(III) monomers, connecting them through a Mn-NC-Fe-CN-Mn bridge (Scheme 1).

Structure of Complex [Mn(L)(H_2O)Cl] (1). The mononuclear complex **1** crystallizes in the orthorhombic centrosymmetric space group P_{bca}. The asymmetric unit contains one mononuclear unit, which contains one Mn(III) ion, one deprotonated ligand L^{2-}, one coordinated Cl^-, and one coordinated water molecule (Figure 1).

Selected coordination bond distances and angles are given in Table S1 in the Supporting Information. The metal center shows a distorted octahedral geometry. As observed in other N_2O_2 donor Schiff base-metal complexes, the four equatorial positions are occupied by the four donor atoms (N1, N2, O1, and O2) of the Schiff base while the *trans*-axial sites are occupied by one chloride ion (Cl1) and one water molecule (O1W). The Mn−O and Mn−N bond lengths of the Schiff-base donor atoms are in the normal range: Mn1−O1 = 1.881(4) Å, Mn1−O2 = 1.863(4) Å, Mn1−N1 = 1.979(4) Å, and Mn1−N2 = 1.973(4) Å, whereas the axial bond lengths are comparatively longer: Mn1−Cl1 = 2.554(2) Å and Mn1−O1W = 2.287(3) Å. These distances reflect the expected Jahn−Teller elongation along the axial bonds. The Mn center is displaced toward the Cl1 atom ∼0.073 Å from the mean plane formed by the donor atoms (O1−N1−N2−O2) of the Schiff-base ligand.

Supramolecular structural analysis reveals that two neighboring mononuclear units are connected in an antiparallel fashion by $\pi-\pi$ interactions to form a supramolecular dimer, which is further stabilized by a double O1W−H1W1···O1 hydrogen-bonding interaction (Figure 2). These dimers are bridged by O1W−H2W1···Cl1 hydrogen-bonding interactions to form supramolecular layers parallel to the crystallographic *ab*-plane (Figure S1 in the Supporting Information). These supramolecular layers are further bridged by C8−H8A···Cl1 and C15−H15···Cl1 hydrogen-bonding interactions to develop a 3D supramolecular structure (Figure S2). The hydrogen bonding and $\pi-\pi$ interaction parameters are summarized in Tables S2 and S3 in the Supporting Information.

Crystal Structure of $(H_3O)[Mn(L)(H_2O)_2]\{[Mn(L)(H_2O)]_2Fe(CN)_6\}\cdot 4H_2O$ (2). Single-crystal X-ray analysis reveals that this compound crystallizes in the centrosymmetric triclinic $P\bar{1}$ space group. It is a 1:1 cocrystal of a Mn_2Fe trimer and a Mn(III) monomer. The asymmetric unit contains one monomeric unit, two halves trimeric units, one oxonium cation, and four disordered guest water molecules (Figure 3). The trimeric unit is dianionic and its charge is balanced by the monocationic monomer and one oxonium ion. Note that the presence of the oxonium cation is not only established by charge balance requirements but also by the X-ray crystal data that shows three H atoms around the O5W atom with the expected trigonal pyramidal geometry with similar H−O−H bond angles of 104.4°, 104.6°, and 105.1°. The crystallographic data is presented in Table 1, and some selected coordination bond lengths and angles are summarized in Table S4 in the Supporting Information. The cocrystal contains two different trimeric units. Each trimeric unit is formed by two Mn(III)-Schiff base complexes connected through two *trans* cyanide groups of the hexacyanoferrate(II) unit that acts as a linear bridge, replacing the chloride groups in the original monomeric complex **1**. Interestingly, the water molecule remains coordinated with the Mn(III) ions, precluding the formation of an alternating cyanide-bridged Mn(III)−Fe(II)

https://dx.doi.org/10.1021/acs.inorgchem.0c00909
Inorg. Chem. XXXX, XXX, XXX−XXX

Scheme 1. Complete Synthetic Scheme of the Ligand (H_2L) and Complexes 1 and 2

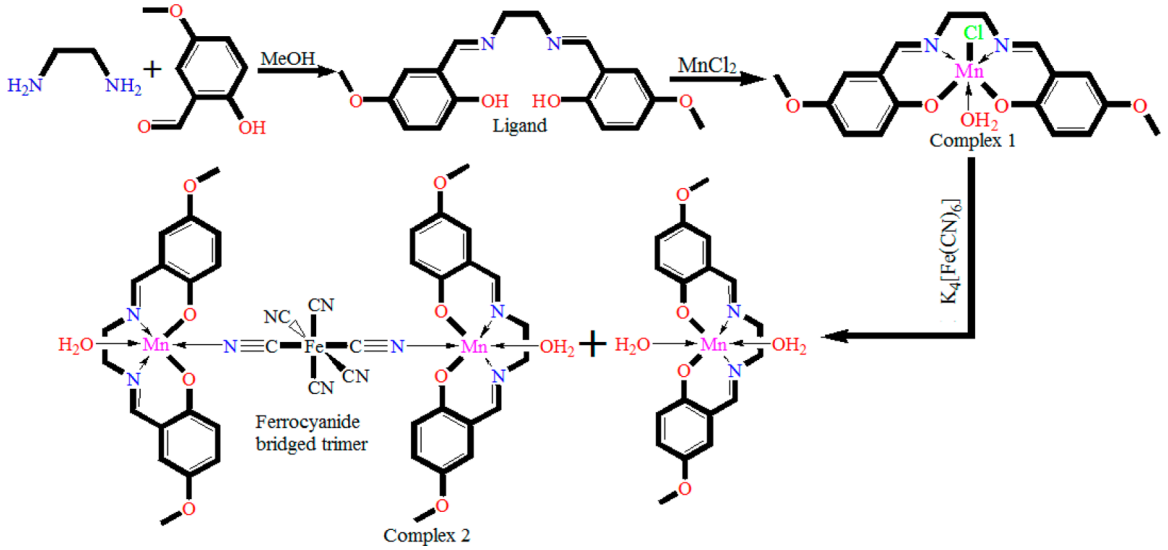

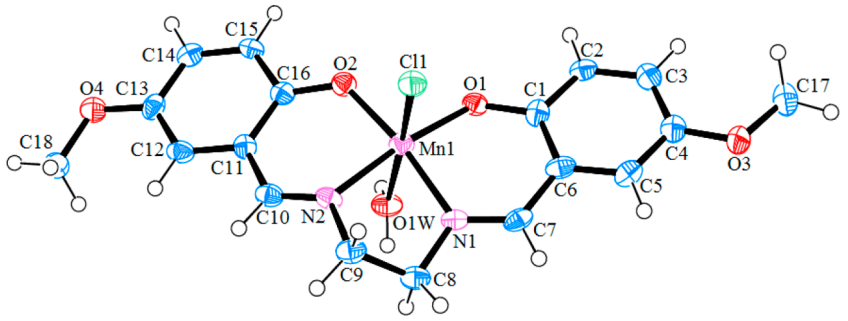

Figure 1. ORTEP diagram and labeling scheme of complex **1** with 30% ellipsoid probability.

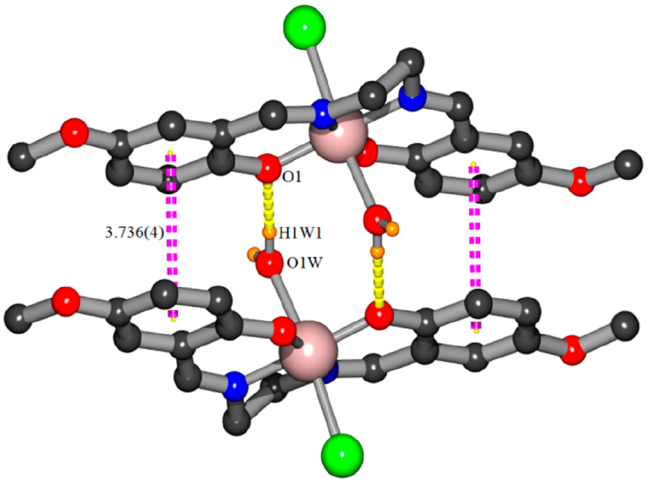

Figure 2. Supramolecular dimer formation with $\pi-\pi$ and O1W–H1W1···O1 hydrogen-bonding interactions in complex **1**.

chain. In each trimer, the asymmetric unit contains a full Mn(III)-Schiff base complex moiety and half $[Fe(CN)_6]^{4-}$ unit. In both trimers the Mn(III) ions show a distorted octahedral geometry where the four equatorial positions are occupied by the four donor sites of the Schiff base ligands and the axial positions are occupied by a water molecule and N atom of the CN group of the bridging $[Fe(CN)_6]^{4-}$ unit (Figure 3). In both trimers, the bond lengths from the N_2O_2 Schiff-base donor atoms to the metal centers are quite similar: Mn1–O1 = 1.862(5) Å, Mn1–O2 = 1.889(5) Å, Mn1–N1 = 1.981(6) Å, and Mn1–N2 = 1.985(6) Å for trimer **1** and Mn2–O5 = 1.872(5) Å, Mn2–O6 = 1.902(5) Å, Mn2–N6 = 1.977(6) Å, and Mn2–N7 = 1.997(6) Å for trimer **2**. In both trimers, the two axial bond lengths are longer than the equatorial ones: Mn1–O1W = 2.290(5) Å and Mn1–N3 = 2.316(6) Å in trimer **1** and Mn2–O2W = 2.294(5) Å and Mn2–N8 = 2.2478(6) Å in trimer **2**, indicating the presence of a Jahn–Teller elongation in both trimers, as observed in complex **1** (see above). The trimers are not linear, since the Mn–N≡C bond angles are 143.38° and 145.01° in trimers **1** and **2**, respectively.

In the monomeric unit, the metal ion (Mn3) also shows a distorted octahedral geometry, as in complex **1**. The Schiff base occupies the four equatorial coordination sites, using its four donor sites (O9, O10, N11, and N12). The corresponding bond lengths are similar to those observed in compound **1** and in both trimers in compound **2**: Mn3–O9 = 1.874(5) Å, Mn3–N12 = 1.984(6) Å, Mn3–O10 = 1.894(6) Å, and Mn3–N11 = 1.988(6) Å. In contrast to complex **1**, the two axial sites are occupied by two water molecules (O3W and O4W). As expected, the axial Mn–O bond lengths: Mn3–O3W = 2.299(6) Å and Mn3–O4W = 2.215(5) Å are longer than the equatorial ones, showing, once more, the existence of a Jahn–Teller elongation in the Mn(III)-monomeric unit. The Mn3 center is displaced toward the O4W molecule by ∼0.043 Å from the mean equatorial plane.

https://dx.doi.org/10.1021/acs.inorgchem.0c00909
Inorg. Chem. XXXX, XXX, XXX–XXX

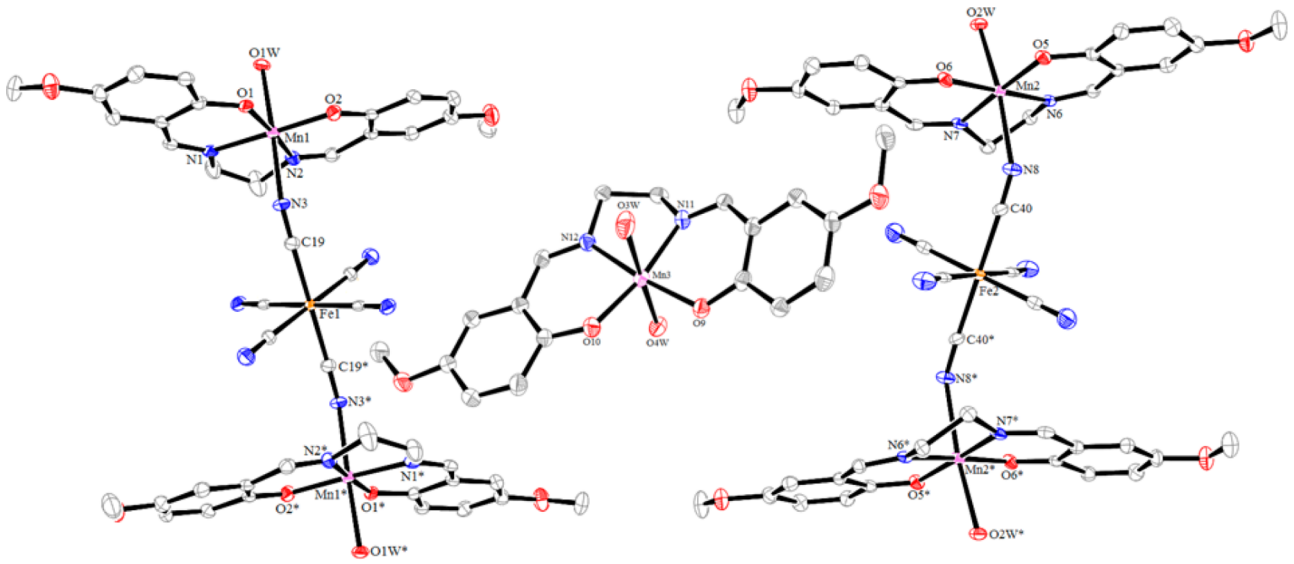

Figure 3. ORTEP diagram in **2** showing two complete trimers and a monomer with atom labeling. The solvent molecules, oxonium cation, and H atoms are omitted for clarity. Ellipsoids drawn at 15% probability.

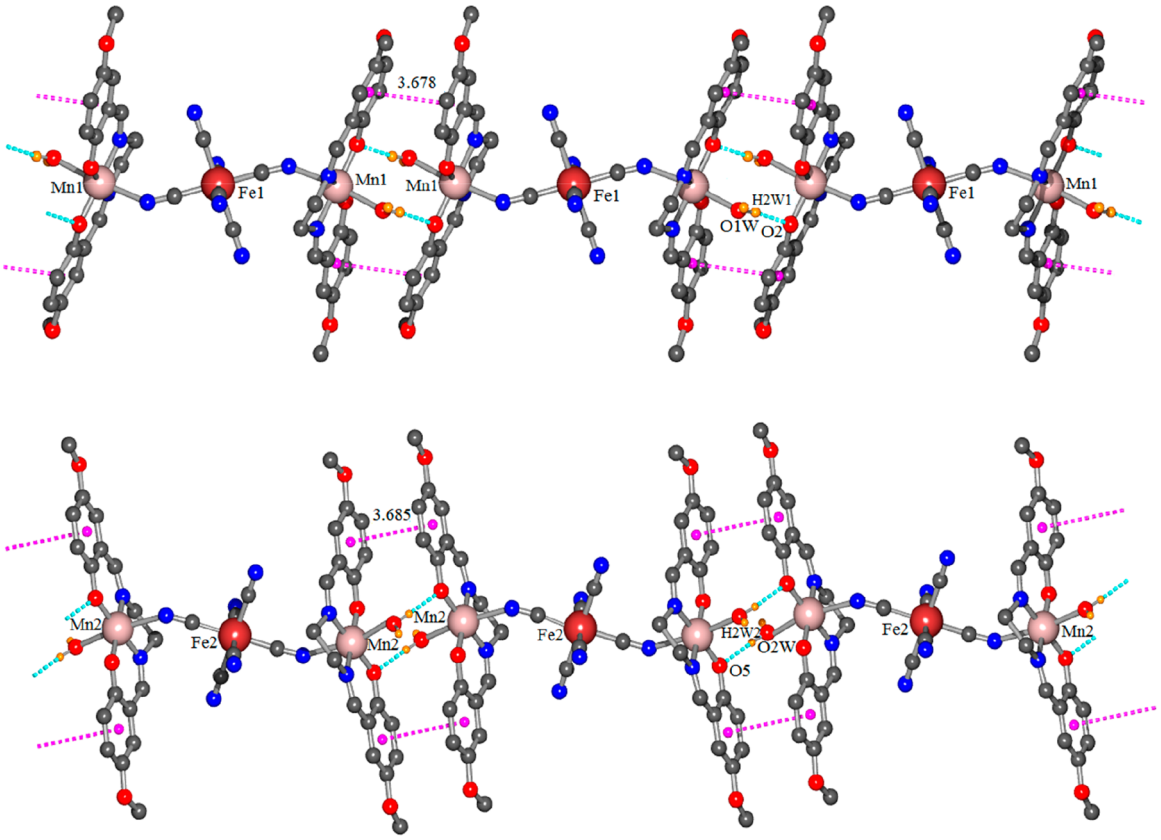

Figure 4. View of the chains of trimers Mn1−Fe1−Mn1 (top) and Mn2−Fe2−Mn2 (bottom), showing the centroids of the aromatic rings of the ligands (as pink spheres) and the shortest C_g−C_g distances (as pink dotted lines). Hydrogen bonds are indicated as light blue dotted lines.

Supramolecular structural analysis reveals that each trimeric unit is connected by hydrogen bonding interactions implying the coordinated water molecules and by π−π interactions to form supramolecular chains parallel to the crystallographic *b*-axis. Each independent trimer forms a different type of supramolecular chain (Figure 4). These two different chains are arranged parallel and are connected by O2W−H1W2···N4 and O1W−H1W1···N10 hydrogen-bonding interactions to form a supramolecular layer in the *ab*-plane.

The cations (the monomeric Mn(III) complex and the oxonium ions) and the disordered solvent molecules are located in the interlayer space. These molecules and ions are connected with the anionic supramolecular layers by means of hydrogen-bonding interactions. All these supramolecular

https://dx.doi.org/10.1021/acs.inorgchem.0c00909
Inorg. Chem. XXXX, XXX, XXX−XXX

interactions are summarized in Tables S5 and S6 in the Supporting Information.

Theoretical DFT Study of Noncovalent Interactions. To highlight the behavior of compounds **1** and **2** commented above and the easy replacement of the chloride ligand by the hexacyanoferrate(II) unit, we have performed DFT calculations at the PBE1PBE-D3/def2-TZVP level of theory (see the Theoretical Methods section for details). First, we have compared the hydrogen-bonded dimerization energy of the supramolecular dimer shown in Figure 2 to the dissociation energy of the Mn(III)-Cl coordination bond. The interaction energy of the dimer of compound **1**, along with the QTAIM distribution of bond critical points and bond paths, are given in Figure 5. It can be observed that the dimerization energy is

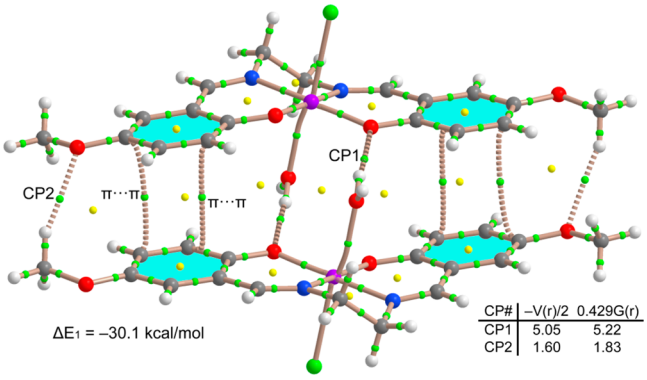

Figure 5. AIM distribution of bond and ring critical points (green and yellow spheres, respectively) and bond paths obtained for the self-assembled dimer of compound **1**. The dissociation energies of the hydrogen bonds using the $V(r)$ and $G(r)$ values at the bond CP are indicated in (kcal/mol) at the lower-right corner and the formation energy of the assembly (ΔE_1) is also given near the assembly.

very large (ΔE_1 = −30.1 kcal/mol), because of the cooperative formation of several O···H and C−H···O hydrogen bonds and $\pi-\pi$ interactions, which are characterized by the corresponding bond critical points (CPs) and bond paths interconnecting the interacting atoms. In order to measure the contribution of the hydrogen bonds, we have used the AIM energy densities at the bond CPs. This methodology has been effectively used by us and others to analyze several types of noncovalent interactions.[46−48] The dissociation energy of each hydrogen-bonding contact can be estimated according to the approach proposed by Espinosa et al.[49] and Vener et al.,[50] which developed energy descriptors specifically for hydrogen bonds. Figure 5 also shows the dissociation energy (in kcal/mol) obtained for each hydrogen bond using both indicators, i.e., the potential energy density $V(r)$ and the Lagrangian kinetic energy $G(r)$. The energies are indicated in Figure 5, and they evidence that the contribution of both O−H···O hydrogen bonds is ∼10.4 kcal/mol and that of the C−H···O bonds involving the methoxide groups is significantly smaller (i.e., 3.6 kcal/mol), using the $G(r)$ descriptor. Therefore, the contribution of the π-stacking and other long-range van der Waals interactions is very significant (∼16 kcal/mol). The dissociation energy of the Mn(III)−Cl coordination bond computed for **1** in MeOH at the same level of theory is −29.3 kcal/mol, which is slightly weaker that the dimerization energy.

We have also evaluated the reaction energy of the transformation depicted in Scheme 2 in order to rationalize the transformation of compound **1** to compound **2** upon the addition of hexacyanoferrate(II). Fortunately, the energy of formation of **2** from **1** is strongly favored (ΔE_r = −19.7 kcal/mol), using methanol as the solvent in the calculation. Note that this reaction energy does not compensate for the energy of the hydrogen-bonded dimer formation of **1** observed in the solid state (ΔE_1; see Figure 5). However, this matter is not important, because the same combination of interactions is also found in the solid state of compound **2**, as detailed in the supramolecular polymers shown in Figure 4. We have performed the QTAIM analysis of a dimeric model of the polymer that is shown in Figure 6, and exactly the same distribution of critical points and bond paths is obtained. It is also worthwhile to comment that the O−H···O hydrogen bonds in **2** are even stronger than those in compound **1**.

Taken together, the results from the theoretical DFT study of complexes **1** and **2** revealed that the ligand exchange of Cl^- by $[Fe(CN)_6]^{4-}$ is energetically favored and preferred over the water substitution since the Mn−Cl coordination bond is weaker than the strength of the weak interactions involved in the formation of the dimer/polymers (hydrogen bonds and $\pi-\pi$ interactions).

Magnetic Properties of Compound 1. At room temperature, the $\chi_m T$ value per Mn(III) ion for compound **1** is ca. 3.0 cm^3 K mol^{-1}, which is close to the expected value for an isolated Mn(III) ion with a ground spin state of S = 2 and a g-value close to 2. When the sample is cooled, $\chi_m T$ remains constant, down to ca. 20 K, and shows a sharp decrease at lower temperatures to reach a value of ca. 0.8 cm^3 K mol^{-1} at 2 K (Figure 7), which suggests the presence of a weak antiferromagnetic interaction in **1** and/or the presence of a zero field splitting in the Mn(III) ions. Since the structure of this compound indicates the presence of quasi-isolated Mn(III) monomers, we have fit the magnetic properties to a

Scheme 2. Transformation from 1 to 2 is Energetically Favorable in Methanol Medium

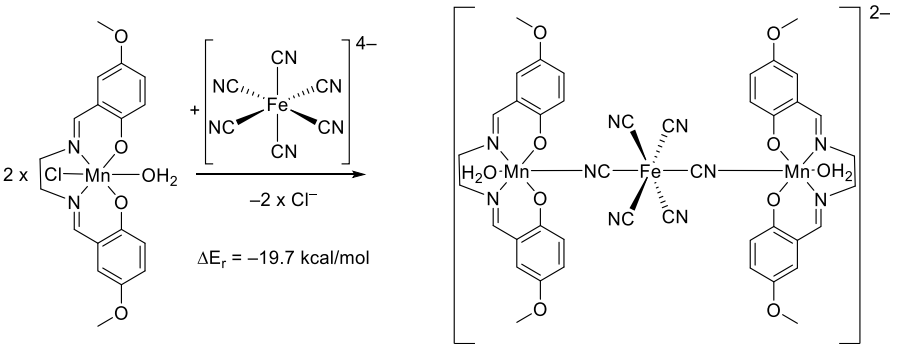

https://dx.doi.org/10.1021/acs.inorgchem.0c00909
Inorg. Chem. XXXX, XXX, XXX−XXX

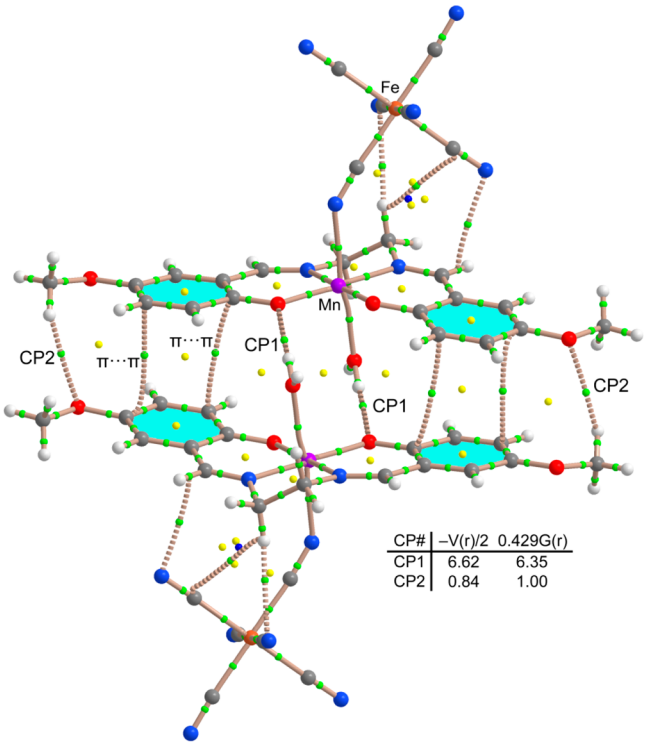

Figure 6. AIM distribution of bond and ring critical points (green and yellow spheres, respectively) and bond paths obtained for a model dimer of compound **2**. The dissociation energies of the hydrogen bonds using the $V(r)$ and $G(r)$ values at the bond CP are indicated in (kcal/mol) in the lower-right corner.

simple model considering an isolated $S = 2$ ion with a zero field splitting (ZFS) to account for the sharp decrease in $\chi_m T$ at low temperatures, using the program PHI.[51] This model reproduces very satisfactorily the magnetic properties of complex **1** in the entire temperature range with $g = 1.958$ and $|D| = 0.69$ cm^{-1} with a residual of 0.0679 (see the dotted line in Figure 7).

Although the magnetic fitting to a monomer with a ZFS produces very satisfactory results, and we have also considered the possible presence of a weak intermolecular interaction through the $\pi-\pi$ and hydrogen-bonding interactions. This weak intermolecular coupling is supported by the presence of a maximum at very low temperatures in the χ_m vs T plot (Figure 7b). Thus, if we include the presence of a weak intermolecular coupling with the mean field approximation (zJ), we can replicate even better the magnetic properties of compound **1** with $g = 1.959$, $zJ = -0.03$ cm^{-1}, and $|D| = 1.23$ cm^{-1} with a residual of 0.0158 (solid line in Figure 7). As expected, the interaction between the Mn(III) centers is weak and antiferromagnetic, since usually $\pi\cdots\pi$ interactions give rise to weak couplings.[52−57] On the other side, the D value found for the isolated Mn(III) center is quite low and is in the typical range observed (−3.8 cm^{-1} to +3.1 cm^{-1}) for mononuclear Mn(III) ions.[58]

Further confirmation of the presence of a very weak antiferromagnetic intermolecular interaction is provided by the isothermal magnetization at 2 K of compound **1** (Figure 8a). This measurement shows a sigmoidal shape with a maximum slope at ca. 2.0 T, as can be found in the derivative of the M vs H plot (Figure 8b), which suggests that **1** is a metamagnet with a critical field of ca. 2.0 T at 2 K (i.e., the weak antiferromagnetic coupling can be cancelled by applying a high magnetic field, above ca. 2.0 T, giving rise to a ferromagnetic coupling). Therefore, we can confirm that there is a very weak antiferromagnetic intermolecular interaction when the applied magnetic field is below ca. 2.0 T.

A further confirmation of this metamagnetic behavior is represented by the thermal variation of χ_m for different applied fields (Figure 9). As can be seen, χ_m shows a maximum at very low temperatures when the applied field in below ca. 2.0 T and the maximum disappears for fields above 2.0 T, in agreement with the isothermal magnetization measurements.

Magnetic Properties of Complex 2. The room-temperature value of $\chi_m T$ per formula unit (i.e., three Mn(III) ions and a Fe(II) ion) is ca. 9.0 cm^3 K mol^{-1} (Figure 10a). This value is close to the expected one for three $S = 2$ Mn(III) with $g = 2$ and indicates that the Fe(II) ion is a diamagnetic low spin Fe(II) ion (as expected for a Fe(II) coordinated to six strong-field CN ligands). When the temperature is reduced, $\chi_m T$ remains the same up to ca. 25 K, and below this temperature, it shows a progressive decrease to ca. 1.1 cm^3 K mol^{-1} at 2 K (see inset in Figure 10a). This behavior suggests the presence of a weak antiferromagnetic interaction in compound **2** and/or the presence of a zero field splitting in the Mn(III) ions. As observed in compound **1**, the thermal variation of χ_m shows a maximum at ca. 6 K (Figure 10b), suggesting that there is also a very weak antiferromagnetic coupling in compound **2**.

A detailed study of the structure of compound **2** indicates that the Mn(III) monomeric units are well-isolated but each Mn_2Fe trimer presents two short intertrimer $\pi\cdots\pi$ interactions and two hydrogen bonds with its two neighboring trimers to generate a regular chain of trimers (Figure 4). Nevertheless, since the Fe(II) ions are diamagnetic, the chains can be considered, from the magnetic point of view, as isolated Mn(III)−Mn(III) dimers. Note that since the two C_g-C_g distances and the hydrogen-bonding parameters are very similar in both chains (see Tables S5 and S6 in the Supporting

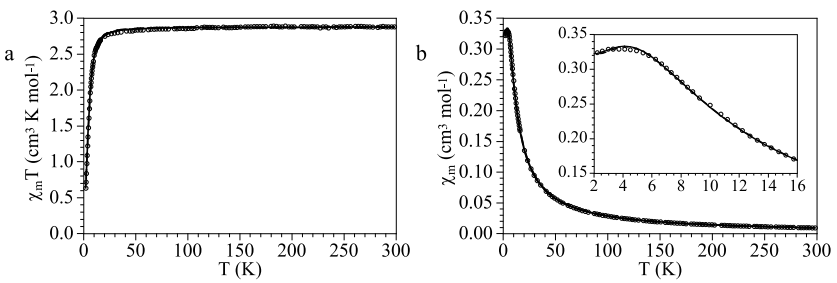

Figure 7. Thermal variation of (a) $\chi_m T$ and (b) χ_m for compound **1**. Solid and dotted lines represent the best fit to the models (see text).

https://dx.doi.org/10.1021/acs.inorgchem.0c00909
Inorg. Chem. XXXX, XXX, XXX−XXX

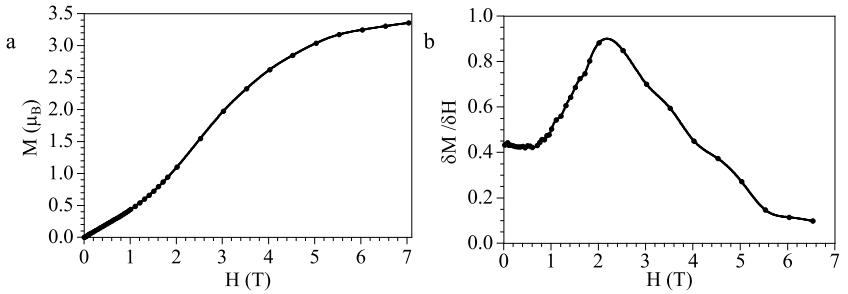

Figure 8. (a) Isothermal magnetization at 2 K for compound **1**. (b) Derivative of the magnetization, as a function of the magnetic field, showing a broad maximum at ca. 2.0 T.

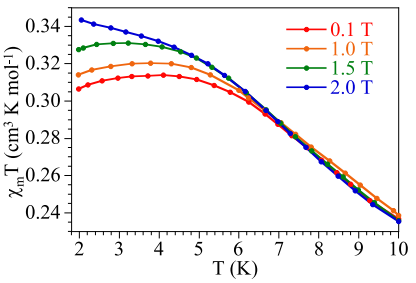

Figure 9. Thermal variation of χ_m for compound **1** in the low-temperature region with different applied fields.

Information), we can consider that the Mn(III)−Mn(III) coupling is the same in both chains.

Accordingly, we have fit the magnetic properties to a model of an isolated $S = 2$ ion with a ZFS plus a $S = 2$ dimer with a weak antiferromagnetic coupling (J) and a ZFS utilizing the program PHI.[43] In order to decrease the quantity of adjustable parameters, we have assumed that both Mn(III) dimers (Mn1−Mn1 and Mn2−Mn2) have the same coupling constant (J) and that all the Mn(III) ions have the same g- and D-values. This model reproduces very effectively the magnetic properties of compound **2** in the entire temperature range with $g = 2.009$, $|D| = 1.21$ cm^{-1}, and $J = -0.42$ cm^{-1}, with a residual of 0.1355 (solid lines in Figure 10; the exchange Hamiltonian is written as $H = -JS_1S_2$). As observed for compound **1**, the magnetic interaction between the Mn(III) centers is weak and antiferromagnetic, as expected for $\pi\cdots\pi$ interactions.[44−49] Again, the D value found is low and is within the typical range observed (−3.8 cm^{-1} to +3.1 cm^{-1}) for Mn(III) ions.[50]

An additional confirmation of the presence of an antiferromagnetic interaction in compound **2** is also given by the isothermal magnetization at 2 K (Figure 11a). This plot shows a sigmoidal shape with a maximum slope at ca. 2.5 T, as deduced from the maximum of the derivative (Figure 11b), suggesting that compound **2** also behaves as a metamagnet.

To confirm this metamagnetic behavior, we have also measured the magnetic susceptibility with different applied fields in the low-temperature region (see Figure 12). These measurements show the presence of a maximum in χ_m at low temperatures (∼6 K) that shifts to lower temperatures as the applied field increases and finally disappears for fields above 2.5 T, confirming that compound **2** is a metamagnet with a critical field of ca. 2.5 T.

CONCLUSIONS

In this work, we have presented a unique example of an inorganic reaction where a metal−ligand bond undergoes dissociation helped by the formation of intermolecular $\pi-\pi$ and hydrogen-bonding interactions. DFT calculations at the PBE1PBE-D3/def2-TZVP level confirm that the summation of the energies of all these intermolecular interactions surpasses the metal−ligand one. This fact has allowed us to prepare a trimeric molecular metamagnet from a monomeric metamagnetic precursor for the first time.

Thus, we present the formation of a novel Schiff-base ligand (H_2L) and the use of this ligand to prepare a Mn(III) monomer that exhibits very weak antiferromagnetic coupling through intermolecular $\pi-\pi$ and hydrogen-bonding interactions. This weak antiferromagnetic interaction can be cancelled out by the application of an external magnetic field, giving rise to a metamagnetic behavior with a critical field of ca. 2.0 T at 2 K. Combination of this Mn(III) monomer with $[Fe(CN)_6]^{4-}$ generates a Mn_2Fe trimer where the diamagnetic $[Fe(CN)_6]^{4-}$ complex acts as a linear connector between two monomeric Mn(III) complexes. These anionic trimers crystallize with a cationic Mn(III) monomer (closely related to the precursor monomer) in a 1:1 cocrystal to form compound **2**. The trimers are further assembled by $\pi-\pi$ and hydrogen-bonding

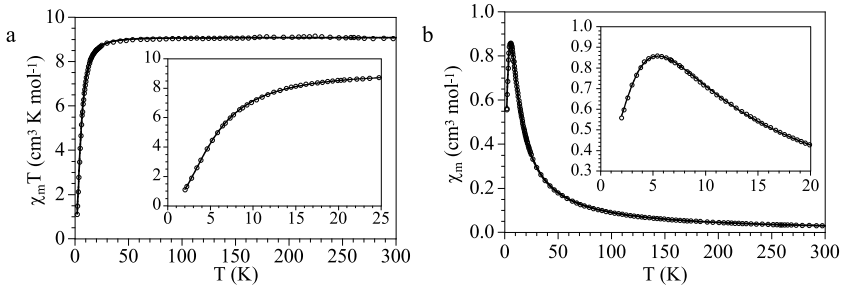

Figure 10. Thermal variation of (a) $\chi_m T$ and (b) χ_m for compound **2**. Insets show the low-temperature regions. Solid lines are the best fit to the model (see text).

https://dx.doi.org/10.1021/acs.inorgchem.0c00909
Inorg. Chem. XXXX, XXX, XXX−XXX

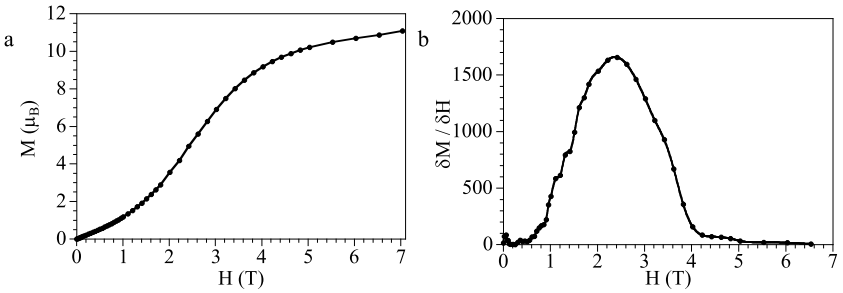

Figure 11. (a) Isothermal magnetization at 2 K for compound **2**. (b) Derivative of the magnetization *M*, as a function of *H*, showing a broad maximum at ca. 2.5 T.

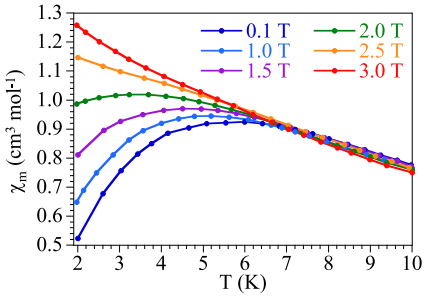

Figure 12. Thermal variation of χ_m for compound **2** in the low-temperature region with different applied fields.

interactions to build 1D supramolecular chains. Compound **2** also behaves as a metamagnet with a slightly higher critical field of ca. 2.5 T at 2 K. The magnetic behavior of both compounds has been reproduced with a simple model of a S = 2 monomer with a ZFS and a very weak intermolecular interaction (for **1**) and a S = 2 monomer with ZFS plus an antiferromagnetically coupled S = 2 dimer with a ZFS (for **2**). Finally, we hope that such study will help to analyze several biological processes, such as oxygen transport by hemoglobin and myoglobin, different metallo-enzymatic catalysis, etc.

■ ASSOCIATED CONTENT

Supporting Information

The Supporting Information is available free of charge at https://pubs.acs.org/doi/10.1021/acs.inorgchem.0c00909.

Figures showing the packing of compound, tables with bond distances, angles, and intermolecular interaction parameters for compounds **1** and **2** (PDF)

Accession Codes

CCDC 1994095 and 1991670 contain the crystallographic data of compounds **1** and **2**, respectively. This data can be obtained free of charge via http://www.ccdc.cam.ac.uk/conts/retrieving.html, or from the Cambridge Crystallographic Data Centre, 12 Union Road, Cambridge CB2 1EZ, UK; fax: (+44) 1223−336−033; or e-mail: deposit@ccdc.cam.ac.uk.

■ AUTHOR INFORMATION

Corresponding Authors

Rajat Saha − *Department of Physics, Jadavpur University, Kolkata 700032, India; Department of Chemistry, Kazi Nazrul University, Asansol 713340, WB, India;* orcid.org/0000-0003-1943-3650; Email: rajat.saha@knu.ac.in

Sanjay Kumar − *Department of Physics, Jadavpur University, Kolkata 700032, India;* orcid.org/0000-0002-0584-0901; Email: kumars@phys.jdvu.ac.in

Subrata K. Dey − *Department of Chemistry, Sidho-Kanho-Birsha University, Purulia 723104, WB, India;* Email: skdusask@yahoo.ca

Carlos J. Gómez García − *Departamento de Química Inorgánica, CMol. Universidad de Valencia, 46980 Paterna, Valencia, Spain;* orcid.org/0000-0002-0015-577X; Email: carlos.gomez@uv.es

Authors

Somen Goswami − *Department of Physics, Jadavpur University, Kolkata 700032, India*

Soumen Singha − *Department of Physics, Jadavpur University, Kolkata 700032, India*

Indrajit Saha − *Department of Chemistry, RKMRC, Narendrapur 700103, WB, India*

Abhishikta Chatterjee − *Department of Chemistry, Sidho-Kanho-Birsha University, Purulia 723104, WB, India*

Antonio Frontera − *Departament de Química, Universitat de les Illes Balears, 07122 Palma de Mallorca, Baleares, Spain;* orcid.org/0000-0001-7840-2139

Complete contact information is available at: https://pubs.acs.org/10.1021/acs.inorgchem.0c00909

Author Contributions

The manuscript was written through contribution of all authors. All authors have given approval to the final version of the manuscript.

Notes

The authors declare no competing financial interest.

■ ACKNOWLEDGMENTS

R. S. acknowledges SERB, Government of India for SERB-TARE project (File No: TAR/2018/000744). We thank the Spanish MINECO (ProjectNo. CTQ2017-87201-P AEI/FEDER, UE) and the Generalidad Valenciana (Prometeo/2019/076 project) for financial support.

■ REFERENCES

(1) Turro, N. J. Supramolecular organic photochemistry: Control of covalent bond formation through non-covalent supramolecular interactions and magnetic effects. *Proc. Natl. Acad. Sci. U. S. A.* **2002**, *99*, 4805−4809.

(2) Desiraju, G. R. Chemistry beyond the molecule. *Nature* **2001**, *412*, 397−400.

(3) Merlau, M. L.; del Pilar Mejia, M.; Nguyen, S. T.; Hupp, J. T. Artificial Enzymes Formed through Directed Assembly of Molecular Square Encapsulated Epoxidation Catalysts. *Angew. Chem., Int. Ed.* **2001**, *40*, 4239−4242.

https://dx.doi.org/10.1021/acs.inorgchem.0c00909
Inorg. Chem. XXXX, XXX, XXX−XXX

(4) Leung, D. H.; Fiedler, D.; Bergman, R. G.; Raymond, K. N. Selective C-H Bond Activation by A Supramolecular Host−Guest Assembly. *Angew. Chem., Int. Ed.* **2004**, *43*, 963−966.
(5) Jun, C.-H. Transition Metal-Catalyzed Carbon−Carbon Bond Activation. *Chem. Soc. Rev.* **2004**, *33*, 610−618.
(6) Annamalai, L.; Liu, Y.; Deshlahra, P. Selective C−H Bond Activation via NO_x-Mediated Generation of Strong H-Abstractors. *ACS Catal.* **2019**, *9*, 10324−10338.
(7) Della Ca', N.; Fontana, M.; Motti, E.; Catellani, M. Pd/Norbornene: A Winning Combination for Selective Aromatic Functionalization via C−H Bond Activation. *Acc. Chem. Res.* **2016**, *49*, 1389−1400.
(8) An, K.; Somorjai, G. A. Size and Shape Control of Metal Nanoparticles for Reaction Selectivity in Catalysis. *ChemCatChem* **2012**, *4*, 1512−1524.
(9) Lee, I.; Delbecq, F.; Morales, R.; Albiter, M. A.; Zaera, F. Tuning selectivity in catalysis by controlling particle shape. *Nat. Mater.* **2009**, *8*, 132−138.
(10) Pinter, B.; Van Speybroeck, V.; Waroquier, M.; Geerlings, P.; De Proft, F. Trans Effect and Trans Influence: Importance of Metal Mediated Ligand-Ligand Repulsion. *Phys. Chem. Chem. Phys.* **2013**, *15*, 17354−17365.
(11) Shaw, J. L.; Dockery, C. R.; Lewis, S. E.; Harris, L.; Bettis, R. The Trans Effect: A Guided-Inquiry Experiment for Upper-Division Inorganic Chemistry. *J. Chem. Educ.* **2009**, *86*, 1416−1418.
(12) Pearson, R. G. Hard and soft acids and bases, HSAB, part II, Underlying theories. *J. Chem. Educ.* **1968**, *45*, 643−648.
(13) Cárdenas, C.; Ayers, P. W. How Reliable is The Hard−Soft Acid−Base Principle? An Assessment from Numerical Simulations of Electron Transfer Energies. *Phys. Chem. Chem. Phys.* **2013**, *15*, 13959−13968.
(14) Yu, G.; Jie, K.; Huang, F. Supramolecular Amphiphiles Based on Host−Guest Molecular Recognition Motifs. *Chem. Rev.* **2015**, *115*, 7240−7303.
(15) Haino, T. Molecular-Recognition-Directed Formation of Supramolecular Polymers. *Polym. J.* **2013**, *45*, 363−383.
(16) Li, C. Pillararene-Based Supramolecular Polymers. From Molecular Recognition to Polymeric Aggregates. *Chem. Commun.* **2014**, *50*, 12420−12433.
(17) Roy, B.; Noguchi, T.; Tsuchiya, Y.; Yoshihara, D.; Yamamoto, T.; Shinkai, S. Molecular Recognition Directed Supramolecular Control Over Perylene-Bisimide Aggregation Resulting in Aggregation Induced Enhanced Emission (AIEE) and Induced Chiral Amplification. *J. Mater. Chem. C* **2015**, *3*, 2310−2318.
(18) Fiedler, D.; Leung, D. H.; Bergman, R. G.; Raymond, K. N. Selective Molecular Recognition, C-H Bond Activation, and Catalysis in Nanoscale Reaction Vessels. *Acc. Chem. Res.* **2005**, *38*, 349−358.
(19) Zhang, X.-M.; Wang, Y.-Q.; Wang, K.; Gao, E.-Q.; Liu, C.-M. Metamagnetism and Slow Magnetic Dynamics in An Antiferromagnet Composed of Cobalt(II) Chains with Mixed Azide−Carboxylate Bridges. *Chem. Commun.* **2011**, *47*, 1815−1817.
(20) Mukherjee, P. S.; Dalai, S.; Chaudhuri, N. R.; Zangrando, E.; Lloret, F. The First Metamagnetic One-Dimensional Molecular Material with Nickel(II) and End-to-End Azido Bridges. *Chem. Commun.* **2001**, 1444−1445.
(21) Zhou, Y. L.; Wu, M. C.; Zeng, M. H.; Liang, H. Magneto-Structural Correlation in A Metamagnetic Cobalt(II)-Based Pillared Trilayer Motif Constructed by Mixed Pyridyl-Type Carboxylate Ligands. *Inorg. Chem.* **2009**, *48*, 10146−10150.
(22) Boeckmann, J.; Wriedt, M.; Nather, C. Metamagnetism and Single-Chain Magnetic Behavior in a Homospin One-Dimensional Iron(II) Coordination Polymer. *Chem. - Eur. J.* **2012**, *18*, 5284−5289.
(23) Sun, W. W.; Tian, Y. C.; Jing, X. H.; Wang, Y. Q.; Gao, E. Q. Solvent-Modulated Metamagnetism in A Nickel(ii) Coordination Polymer with Mixed Azide and Carboxylate Bridges. *Chem. Commun.* **2009**, *31*, 4741−4743.
(24) Motokawa, N.; Matsunaga, S.; Takaishi, S.; Miyasaka, H.; Yamashita, M.; Dunbar, K. R. Reversible Magnetism Between an Antiferromagnet and A Ferromagnet Related to Solvation/Desolvation in A Robust Layered $[Ru_2]_2$TCNQ Charge-Transfer System. *J. Am. Chem. Soc.* **2010**, *132*, 11943−11951.
(25) Sandeman, K. G. Magnetocaloric Materials: The Search for New Systems. *Scr. Mater.* **2012**, *67*, 566−571.
(26) Annaorazov, M. P.; Asatryan, K. A.; Myalikgulyev, G.; Nikitin, S. A.; Tishin, A. M.; Tyurin, A. L. Alloys of The Fe-Rh System As a New Class of Working Material for Magnetic Refrigerators. *Cryogenics* **1992**, *32*, 867−872.
(27) Zeng, M.-H.; Zhang, W.-X.; Sun, X.-Z.; Chen, X.-M. Spin Canting and Metamagnetism in a 3D Homometallic Molecular Material Constructed by Interpenetration of Two Kinds of Cobalt(II) Coordination-Polymer Sheets. *Angew. Chem., Int. Ed.* **2005**, *44*, 3079−3082.
(28) Naiya, S.; Biswas, S.; Drew, M. G. B.; Gomez-García, C. J.; Ghosh, A. A Ferromagnetic Methoxido-Bridged Mn(III) Dimer and a Spin Canted Metamagnetic μ-1,3-Azido-Bridged Chain. *Inorg. Chem.* **2012**, *51*, 5332−5341.
(29) Miyasaka, H.; Clérac, R.; Mizushima, K.; Sugiura, K. I.; Yamashita, M.; Wernsdorfer, W.; Coulon, C. $[Mn_2(saltmen)_2Ni(pao)_2(L)_2](A)_2$ with L = Pyridine, 4-Picoline, 4-*tert*-Butylpyridine, *N*-Methylimidazole and A = ClO_4^-, BF_4^-, PF_6^-, ReO_4^-: A Family of Single-Chain Magnets. *Inorg. Chem.* **2003**, *42*, 8203−8213.
(30) Clérac, R.; Miyasaka, H.; Yamashita, M.; Coulon, C. Evidence for Single-Chain Magnet Behavior in a Mn^{III}−Ni^{II} Chain Designed with High Spin Magnetic Units: A Route to High Temperature Metastable Magnets. *J. Am. Chem. Soc.* **2002**, *124*, 12837−12844.
(31) Miyasaka, H.; Clerac, R.; Wernsdorfer, W.; Lecren, L.; Bonhomme, C.; Sugiura, K.; Yamashita, M. A Dimeric Manganese (III) Tetradentate Schiff Base Complex As a Single-Molecule Magnet. *Angew. Chem., Int. Ed.* **2004**, *43*, 2801−2805.
(32) Lü, Z.; Yuan, M.; Pan, F.; Gao, S.; Zhang, D.; Zhu, D. Syntheses, Crystal Structures, and Magnetic Characterization of Five New Dimeric Manganese(III) Tetradentate Schiff Base Complexes Exhibiting Single-Molecule-Magnet Behavior. *Inorg. Chem.* **2006**, *45*, 3538−3548.
(33) Tandon, S. S.; Thompson, L. K.; Manuel, M. E.; Bridson, J. N. Magnetostructural Correlations in.mu.2−1,1-N_3 Bridged, Dinuclear Copper(II) Complexes. 1. Ferromagnetic and Antiferromagnetic Coupling Associated with the Azide Bridge. *Inorg. Chem.* **1994**, *33*, 5555−5570.
(34) Naiya, S.; Drew, M. G. B.; Diaz, C.; Ribas, J.; Ghosh, A. Synthesis, Crystal Structure, and Magnetic Properties of a Very Rare Double μ-1,1-Azido- and a μ-1,1-(OMe)-Bridged Fe^{III} Dimer Containing a N,N,O-Donor Tridentate Schiff Base Ligand. *Eur. J. Inorg. Chem.* **2011**, *2011*, 4993−4999.
(35) Wang, T.-T.; Bao, S.-S.; Huang, J.; Li, Y.-Z.; Zheng, L.-M. Chiral One-Dimensional O−P−O Bridged $MnII^{I-S}$chiff Base Complexes. *Dalton Trans.* **2013**, *42*, 1842−1847.
(36) Yuan, M.; Gao, S.; Sun, H.-L.; Su, G. An Antiferromagnetic Mn(III) Chain Bridged by Hydrogencyanamide: $[MnIII^{(5\text{-}}$Brsalen)$(\mu 1,3_{\text{-NC}}NH)]n$. *Inorg. Chem.* **2004**, *43*, 8221−8223.
(37) Bain, G. A.; Berry, J. F. Diamagnetic corrections and Pascal's constants. *J. Chem. Educ.* **2008**, *85*, 532−536.
(38) Frisch, M. J.; Trucks, G. W.; Schlegel, H. B.; Scuseria, G. E.; Robb, M. A.; Cheeseman, J. R.; Scalmani, G.; Barone, V.; Petersson, G. A.; Nakatsuji, H.; Li, X.; Caricato, M.; Marenich, A. V.; Bloino, J.; Janesko, B. G.; Gomperts, R.; Mennucci, B.; Hratchian, H. P.; Ortiz, J. V.; Izmaylov, A. F.; Sonnenberg, J. L.; Williams-Young, D.; Ding, F.; Lipparini, F.; Egidi, F.; Goings, J.; Peng, B.; Petrone, A.; Henderson, T.; Ranasinghe, D.; Zakrzewski, V. G.; Gao, J.; Rega, N.; Zheng, G.; Liang, W.; Hada, M.; Ehara, M.; Toyota, K.; Fukuda, R.; Hasegawa, J.; Ishida, M.; Nakajima, T.; Honda, Y.; Kitao, O.; Nakai, H.; Vreven, T.; Throssell, K.; Montgomery, J. A., Jr.; Peralta, J. E.; Ogliaro, F.; Bearpark, M. J.; Heyd, J. J.; Brothers, E. N.; Kudin, K. N.; Staroverov, V. N.; Keith, T. A.; Kobayashi, R.; Normand, J.; Raghavachari, K.; Rendell, A. P.; Burant, J. C.; Iyengar, S. S.; Tomasi, J.; Cossi, M.; Millam, J. M.; Klene, M.; Adamo, C.; Cammi, R.; Ochterski, J. W.; Martin, R. L.; Morokuma, K.; Farkas, O.; Foresman, J. B.; Fox, D. J. *Gaussian 16, Revision A.01*; Gaussian, Inc.: Wallingford, CT, 2016.

https://dx.doi.org/10.1021/acs.inorgchem.0c00909
Inorg. Chem. XXXX, XXX, XXX−XXX

(39) Bader, R. F. W. A Bond Path: A Universal Indicator of Bonded Interactions. *J. Phys. Chem. A* **1998**, *102*, 7314−7323.
(40) Keith, T. A. *AIMAll (Version 13.05.06)*; TK Gristmill Software: Overland Park, KS, 2013.
(41) Sheldrick, G. M. *SHELXS 97, Program for Structure Solution*; University of Göttingen, Göttingen, Germany, 1997.
(42) Sheldrick, G. M. *SHELXL 97, Program for Crystal Structure Refinement*; University of Göttingen, Göttingen, Germany, 1997.
(43) Spek, A. L. Single-crystal structure validation with the program PLATON. *J. Appl. Crystallogr.* **2003**, *36*, 7−13.
(44) Farrugia, L. J. ORTEP-3 for Windows - a version of ORTEP-III with a Graphical User Interface (GUI). *J. Appl. Crystallogr.* **1997**, *30*, 565.
(45) Farrugia, L. J. WinGX suite for small-molecule single-crystal crystallography. *J. Appl. Crystallogr.* **1999**, *32*, 837−838.
(46) Białek, M. J.; Zaręba, J. K.; Janczak, J.; Zoń, J. Chains, Layers, Channels, and More: Supramolecular Chemistry of Potent Diphosphonic Tectons with Tuned Flexibility. The Generation of Pseudopolymorphs, Polymorphs, and Adducts. *Cryst. Growth Des.* **2013**, *13*, 4039−4050.
(47) Mahmoudi, G.; Zaręba, J. K.; Gurbanov, A. V.; Bauzá, A.; Zubkov, F. I.; Kubicki, M.; Stilinović, V.; Kinzhybalo, V.; Frontera, A. Benzyl Dihydrazone versus Thiosemicarbazone Schiff Base: Effects on the Supramolecular Arrangement of Cobalt Thiocyanate Complexes and the Generation of CoN_6 and CoN_4S_2 Coordination Spheres. *Eur. J. Inorg. Chem.* **2017**, *2017*, 4763−4772.
(48) García-Raso, A.; Terrón, A.; López-Zafra, A.; García-Viada, A.; Barta, A.; Frontera, A.; Lorenzo, J.; Rodríguez-Calado, S.; Vázquez-López, E. M.; Fiol, J. J. Crystal Structures of N6-Modified-Amino Acid Related Nucleobase Analogs (II): Hybrid Adenine-*β*-Alanine and Adenine-GABA Molecules. *New J. Chem.* **2019**, *43*, 9680−9688.
(49) Espinosa, E.; Molins, E.; Lecomte, C. Hydrogen Bond Strengths Revealed by Topological Analyses of Experimentally Observed Electron Densities. *Chem. Phys. Lett.* **1998**, *285*, 170−173.
(50) Vener, M. V.; Egorova, A. N.; Churakov, A. V.; Tsirelson, V. G. Intermolecular Hydrogen Bond Energies in Crystals Evaluated Using Electron Density Properties: DFT Computations with Periodic Boundary Conditions. *J. Comput. Chem.* **2012**, *33*, 2303−2309.
(51) Chilton, N. F.; Anderson, R. P.; Turner, L. D.; Soncini, A.; Murray, K. S. PHI. A Powerful New Program for The Analysis of Anisotropic Monomeric and Exchange-Coupled Polynuclear d- and f -block Complexes. *J. Comput. Chem.* **2013**, *34*, 1164−1175.
(52) Wojciechowska, A.; Janczak, J.; Zierkiewicz, W.; Rytlewski, P.; Rojek, T.; Duczmal, M. Copper(II) Complex with L-Arginine - Crystal Sructure, DFT Calculations, Spectroscopic, Thermal and Magnetic Properties. *Mater. Chem. Phys.* **2019**, *228*, 272−284.
(53) Chi, Y.; Shi, J.; Li, H.; Wei, W.; Cottrill, E.; Pan, N.; Chen, H.; Liang, Y.; Yu, L.; Zhang, Y.; Hou, C. pi-pi Stacking, Spin Density and Magnetic Coupling Strength. *Dalton Trans* **2013**, *42*, 15559−15569.
(54) Li, H.; Zhang, S.; Xie, L.; Yu, L.; Shi, J. pi-pi Stacking, Hydrogen Bonding and Anti-Ferromagnetic Coupling Mechanism on A Mononuclear Cu(II) Complex. *J. Coord. Chem.* **2011**, *64*, 1456−1468.
(55) Chi, Y.; Wei, W.; Shi, J.; Zhang, Y.; Liu, S. Intermolecular Interaction and Magnetic Coupling Mechanism Between Adjacent Mononuclear Ni(II) Complexes. *J. Coord. Chem.* **2012**, *65*, 2379−2390.
(56) Sutradhar, M.; Carrella, L. M.; Rentschler, E. Mononuclear Mn(III) and Dinuclear Mn(III,III) Schiff Base Complexes: Influence of *π*−*π* Stacking on Magnetic Properties. *Polyhedron* **2012**, *38*, 297−303.
(57) Chi, Y.; Yu, L.; Shi, J.; Zhang, Y.; Hu, T.; Zhang, G.; Shi, W.; Cheng, P. pi-pi Stacking and Ferromagnetic Coupling Mechanism on A Binuclear Cu(II) Complex. *Dalton Trans* **2011**, *40*, 1453−1462.
(58) Boca, R. Zero-Field Splitting in Metal Complexes. *Coord. Chem. Rev.* **2004**, *248*, 757−815.

https://dx.doi.org/10.1021/acs.inorgchem.0c00909
Inorg. Chem. XXXX, XXX, XXX−XXX